# IONOSPHERIC TEMPORAL-SPATIAL CORRELATION ANALYSIS USING GNSS NETWORKS OVER CHINA

Yan Xiang [1] *, Zhongqi Li[1], Ningbo Wang[2], Ling Pei[1], Wenxian Yu[1]

[1] Shanghai Jiao Tong University, Dongchuan Road 800 Shanghai, China. yan.xiang@sjtu.edu.cn

[2]Aerospace Information Research Institute (AIR), Chinese Academy of Sciences, Beijing, China

**Abstract:**

The Global Navigation Satellite System (GNSS) is well recognized as a valuable tool for studying ionospheric variation, providing a means to measure variations in the Total Electron Content (TEC) of the ionosphere. In this manuscript, we focus specifically on the use of GNSS networks to study ionospheric diurnal variation over China, highlighting some of the key findings and challenges in this area. We begin by describing the basic principles of GNSS-based TEC measurements. We then analyze ionospheric diurnal variation using about 320 GNSS stations in China, including the Southern, Middle, and Northern areas. We also discuss some of the challenges associated with GNSS-based TEC measurement and analysis, such as the effects of receiver and satellite biases and understanding of spatial–temporal TEC variation. Finally, we highlight the sunset enhancement and scintillation of GNSS-based ionospheric diurnal variation research. Overall, this abstract provides a valuable overview of the use of GNSS networks for studying ionospheric diurnal variation and its potential applications for improving space weather forecasting and mitigating the effects of ionospheric disturbances on GNSS-based navigation systems.

**KEY WORDS:** ionospheric delays, sunset effect, sunset enhancement, scintillation, ionospheric temporal-spatial correlation, Equatorial Ionization Anomaly (EIA).

## 1. INTRODUCTION

The ionosphere is the single largest error source to the global navigation satellite system (GNSS) (Xiang et al. 2022). The ionosphere degrades the performance of GNSS basically in two ways. One is the ionospheric delays in GNSS observations. The other one is the ionospheric scintillation. It is no trivial to correct the ionospheric delays under rapid temporal-spatial variations. Rapid variations make it challenging to model the ionospheric delays accurately. Those unmodeled ionospheric residuals reduce the positioning accuracy and make it impossible to obtain ambiguity-fixed solutions for RTK and PPP-RTK (Lyu et al. 2023). The ionospheric scintillation distorts GNSS signals with amplitude and phase fluctuations, which results in frequent cycle slips or loss of lock, lower carrier-noise-ratio, and noisy measurements. Overall, those unmodeled ionospheric delays and ionospheric scintillations affect the resilience of GNSS systems.

Many studies have investigated the ionospheric characteristics and mechanisms that ionosphere affects the performance of GNSS positioning.

Jin et al. (2020) studied the spatial correlation of ionospheric delays based on 24 stations over China in the high solar activity year of 2015. It is suggested that the maximum correlation for the China region is about 1500 km and a decorrelation value of 0.5m to account for the spatial uncertainty.

Similarly, Marini-Pereira et al. (2021) examined the ionospheric spatial error bounds in Brazil based on the grid ionospheric vertical error (GIVE) supporting for the satellite-based augmentation system (SBAS). Results showed that a spatial decorrelation of 1 m for quiet days and 2 m for active days.

Several indicators were developed to monitor the ionospheric scintillation, e.g., S4, PHI, rate of TEC (ROT), detrended IF and single-frequency residuals. The indicators were summarized and compared in Nguyen et al. (2019).

Li et al. (2022) analyzed 1-s and 30-s data on three typical ionospheric irregularities in the year 2014, 2015, and 2017. They found the increasing number of falsely detected cycle slips was responsible for the degradation of PPP performance.

Nie et al. (2022) focused on the high-latitude PPP performance during the March 2015 great geomagnetic storm. They also confirmed that a large number of falsely detected cycle slips. By enlarging the threshold of detecting cycle slip, the kinematic PPP accuracy at high latitudes was significantly improved.

By building the threshold model to detect cycle slips based on the ROT variation to detect the cycle slips correctly, Luo et al. (2022) achieved a 40% improvement in the PPP performance.

However, the latest statistics of ionosphere temporal and spatial correlation over China is less studies. We dedicate to investigating when and where in China are prone to ionospheric unmodeled delays and scintillations in the increasingly 25$^{th}$ solar cycle. We applied the precise slant ionospheric delays extracted from the PPP for data analysis. In addition, we attempt to examine ionosphere dynamics that drives these variations, such as night enhancement, sunset effects, and equatorial ionization anomaly.

The rest of the paper is structured as follows. Section 2 describes the methodology for spatial and temporal correlation analysis. Section 3 displays the preliminary results on the temporal-spatial analysis. Finally, we come to the discussions and conclusions.

* Corresponding author

## 2. METHODOLOGY

This section illustrates the way to derive the ionospheric delay based on the GNSS PPP method. Then the methodology of temporal and spatial correlation analysis is given.

### 2.1 GNSS PPP-based ionospheric delay derivation

The ionospheric TEC measurements based on GNSS raw data can be formulated as:

$$\begin{aligned} \boldsymbol{P_4} &= \boldsymbol{P_2} - \boldsymbol{P_1} \\ &= \boldsymbol{I_2} - \boldsymbol{I_1} + \left(\boldsymbol{b}^r_{P_2} - \boldsymbol{b}^r_{P_1}\right) - \left(\boldsymbol{b}^s_{P_2} - \boldsymbol{b}^s_{P_1}\right) + \sqrt{2}\boldsymbol{\varepsilon_P} \\ &= \boldsymbol{I_2} - \boldsymbol{I_1} + \boldsymbol{DCB}^s_{P1/P2} - \boldsymbol{DCB}^r_{P1/P2} + \sqrt{2}\boldsymbol{\varepsilon_P} \end{aligned} \quad (1)$$

$$\begin{aligned} L_4 &= L_1 - L_2 \\ &= I_2 - I_1 + (\lambda_1 N_1 - \lambda_2 N_2) + \left(b^r_{\Phi_1} - b^r_{\Phi_2}\right) - \left(b^s_{\Phi_1} - b^s_{\Phi_2}\right) + \sqrt{2}\varepsilon_\Phi \\ &= I_2 - I_1 + B_I + DPB^r_{\Phi 1/\Phi 2} - DPB^s_{\Phi 1/\Phi 2} + \sqrt{2}\varepsilon_\Phi \end{aligned} \quad (2)$$

where

$P_j$ is the code measurement at frequency j (j=1, 2) (m), $\Phi_j$ is the carrier phase measurement at frequency j (j=1, 2), $\rho$ is the geometric range between a receiver and a satellite, $c$ is the light speed, $dt^r$ is the receiver clock, $dt^s$ is the satellite clock , $T$ is the slant troposphere delay, $I_1$ is the ionospheric delay along the line-of-sight of receiver and satellite at L1 frequency of $f_1$, $I_2$ is the ionospheric delay at L2 frequency of $f_2$, and $\mathrm{I}_2 = \gamma_2 \mathrm{I}_1$, $\gamma_2 = f_1^2/f_2^2$, $\lambda_j$ is the wavelength at frequency j, $N_j$ is the ambiguity at frequency j (cycle), $b^r_{P_j}, b^s_{P_j}$ are the code biases at frequency j at the receiver and satellite, $\mathrm{b}^{\mathrm{r}}_{\Phi_j}, \mathrm{b}^{\mathrm{s}}_{\Phi_j}$ are the phase biases at frequency j at the receiver and satellite, $\varepsilon_P, \varepsilon_\Phi$ contain the multipath and measurement noise for the code and carrier phase, $I_1 = 40.3 \cdot sTEC/f_1^2$; and $sTEC$ is the slant line-of-sight Total Electron Content.

Typically, the carrier-phase smoothed code method is used for extracting ionospheric delays. The current advanced method to extract the ionospheric observables is estimating the ionospheric measurements together in the precise point positioning (PPP) model (Xiang et al. 2019). The method is superior to the carrier-phase smoothed code method at reducing levelling errors. The line-of-sight ionospheric observables based on PPP are given here as follows.

$$\begin{aligned} L_{UPPP} &= (\gamma_2 - 1)\tilde{I}_1 \\ &= (\gamma_2 - 1)\left(I_1 + \tfrac{1}{\gamma_2 - 1}\left(DCB^s_{P_1/P_2} - DCB^r_{P_1/P_2}\right) + \varepsilon_\Phi\right) \\ &= I_2 - I_1 + \left(DCB^s_{P_1/P_2} - DCB^r_{P_1/P_2}\right) + \varepsilon_\Phi \end{aligned} \quad (3)$$

where

$L_{UPPP}$ is the ionospheric observable based on the UPPP model, $\tilde{I}_1$ the estimated ionospheric observables.

The ionospheric observables based on GNSS are corrupted by frequency- and hardware-related biases, including satellite- and receiver-related biases (Xiang et al. 2020). They must be removed to obtain unbiased and absolute ionospheric delays. Primarily, we correct the satellite-related biases because it is as stable as centimeter-level accuracy. Then we assume that the receiver-related biases are stable in a day. By introducing the GIM, we can calculate a constant daily receiver bias (Montenbruck et al. 2014).

The slant ionospheric delay converts to the vertical delays based on the single-layer assumption, the conversion is shown below.

$$VTEC = STEC/mf \quad (4)$$

where

$$mf = \frac{1}{cos(z')} = \frac{1}{\sqrt{1-\left(\frac{R}{R+h}\right)^2 \cos^2 E}}$$

$VTEC$ is the vertical ionospheric delays, $STEC$ is the slant ionospheric delays, $mf$ is the mapping function, the $z'$ is the zenith angle at the ionospheric pierce point (IPP), E is the elevation, R is the earth radius, h is the ellipsoid height.

### 2.2 Temporal correlation analysis by detrending TEC arcs

We assume that the ionospheric delays change gradually. If there is a sudden increase or random fluctuation, we think there is an anomaly. We applied the sliding window filter to detrend the slow-changing ionospheric delays. The diagram for detrending ionospheric TEC arcs is shown below.

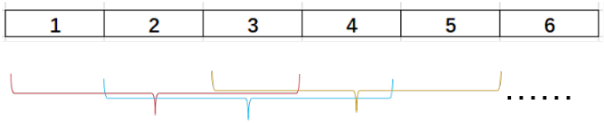


**Figure 1** Diagram for detrending ionospheric TEC arcs based on the sliding window filter.

The sliding window filter method separates the slow temporal changing from the high-frequency component. The temporal remaining high-frequency residuals are visualized to analyze the temporal correlations. The temporal residuals are calculated as:

$$\Delta\mathrm{VTEC}_\mathrm{t} = |VTEC_t - VTEC_{t,window}| \quad (5)$$

where

$\Delta\mathrm{VTEC}_\mathrm{t}$ is the ionospheric temporal residuals; $\mathrm{VTEC}_\mathrm{t}$ is the current VTEC value, $VTEC_{t,window}$ is the VTEC based on the sliding window. It is worth noting that the length of windows matters in terms of the residual scales.

### 2.3 Spatial correlation analysis by calculating distance-dependent TEC residuals

The spatial correlation is often applied to the analysis of distance dependence. By plotting the differences between the ionospheric residuals versus the distance between them, we can observe the spatial correlation between residuals and distances.

The ionospheric spatial residuals for two measurements are defined as

$$\Delta\mathrm{VTEC}_\mathrm{s} = |VTEC_{s,i} - VTEC_{s,j}| \quad (6)$$

where

$\Delta\mathrm{VTEC}_\mathrm{s}$ is the ionospheric spatial residuals, $\mathrm{VTEC}_{\mathrm{s,i}}$ is the VTEC value at the IPP position $i$, $\mathrm{VTEC}_{\mathrm{s,j}}$ is the VTEC value at the IPP position $j$.

## 3. PRELIMINARY RESULTS

Data from about 320 stations distributed over China on a typical day on September 28, 2022, were collected for the temporal and spatial correlation analysis. An elevation cut-off of 40 degrees was chosen to minimize the effects of multipath and the single-layer assumption errors.

### 3.1 Unbiased vertical ionospheric delays

Figure 2 showed the unbiased vertical ionospheric delays from the Northern, Middle, and Southern areas. By comparing the ionospheric delay in the northern region with the ionospheric delay in the southern region, the ionospheric variation of the northern measuring station is more consistent. The amount of ionospheric delay is relatively smaller, about four times smaller.

For the station bjwn with a latitude of around 27 degrees, some of the ionospheric delays are much larger than the other part, almost twice larger. This is because when the satellite signal transmits from the direction of south or low latitude, the signals undergo a larger TEC path. If the signals are from the northern, its ionospheric TEC value is smaller.

The southern station bhhc is roughly at a latitude of about 21 degrees. It can be seen that the time variation curve of ionospheric delay (VTEC) is also more concentrated. The variation of ionospheric delay is more coherent for each satellite than the Middle areas. However, there is an enhancement of the ionospheric delay at the Southern station in the evening around 12:30 UTC (local time (LT) at 20:30), which is associated with the sunset enhancement []. If take a closer look, a disturbance around 15:00 UTC at (23:00 LT), which is the ionospheric scintillation.

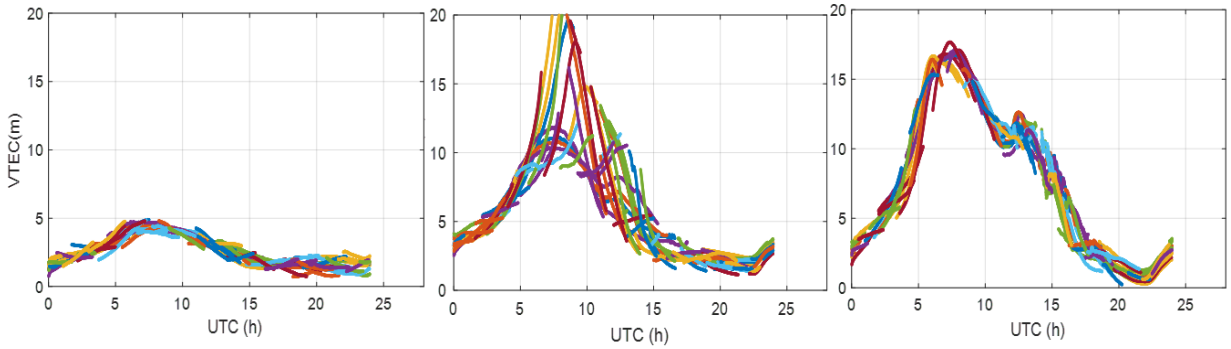


**Figure 2** Vertical ionospheric delays at the typical Northern station alfh (40° N), and Middle station bjwn (27° N), Southern station bhhc (21.5° N).

Figure 3 displays the vertical ionospheric delays over China. Interestingly, the ionospheric delay of satellites coming from the south at mid-latitude stations around 27 degrees is larger than that at low-latitude stations around 20 degrees. This is related to EIA phenomena. The TEC peaks around the geomagnetic latitude of 15 degree, around the geographic latitude of 25 degree, as shown in Figure 3.

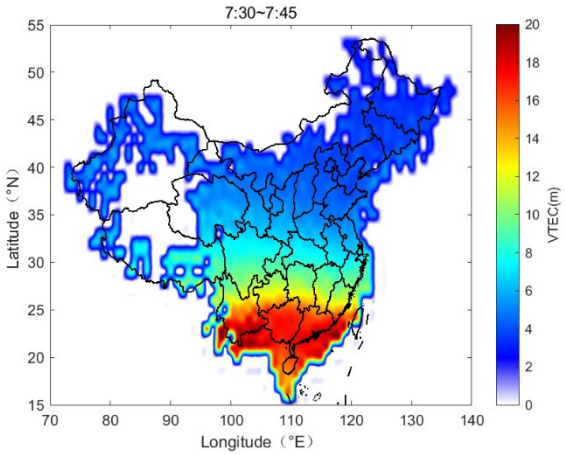


**Figure 3** The geographic distribution of vertical ionospheric delays over China at 7:30 UTC (15:30 LT).

### 3.2 Results on ionospheric temporal analysis

Figure 4 shows the time variations of detrended $\Delta VTEC_t$ for the three stations from the Northern, Middle, and Southern areas. Random fluctuations typically near UTC 15:00. We think the ionospheric scintillation is responsible for the rapid variations. The station at latitude around 27 degree had the most scintillated by the ionosphere. By contrast, there is barely ionospheric scintillation occurs at the northern station and less in the Southern station. Therefore, we think the scintillation is related to the plasma bubble due to the EIA.

The geographic distribution of detrended $\Delta VTEC_t$ around 15 UTC and 23 LT over China is displayed in Figure 5. We also clearly seen that Province Hainan, Guangdong, Guangxi, and Yuannan, which are located at the lower latitude, were more likely to be influenced by the ionospheric irregularity.

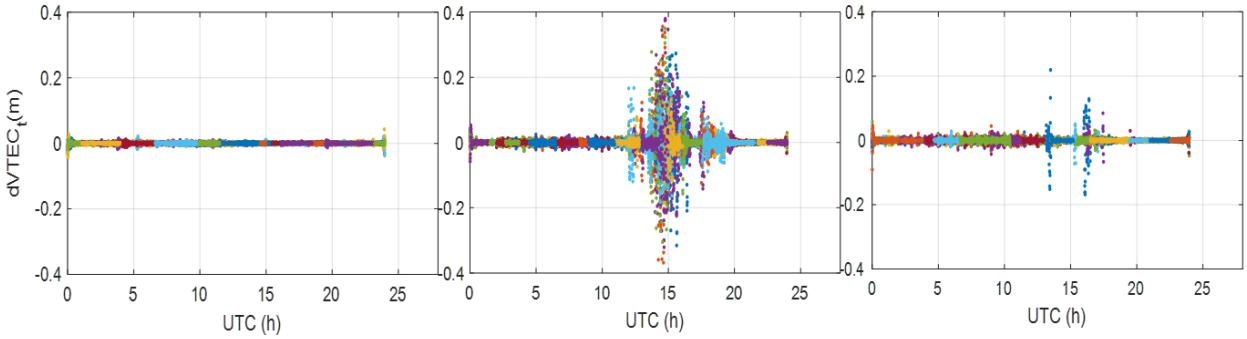


**Figure 4** Detrended vertical ionospheric delays at the typical Northern station alfh (40° N), Middle station bjwn (27° N), Southern station bhhc (21.5° N).

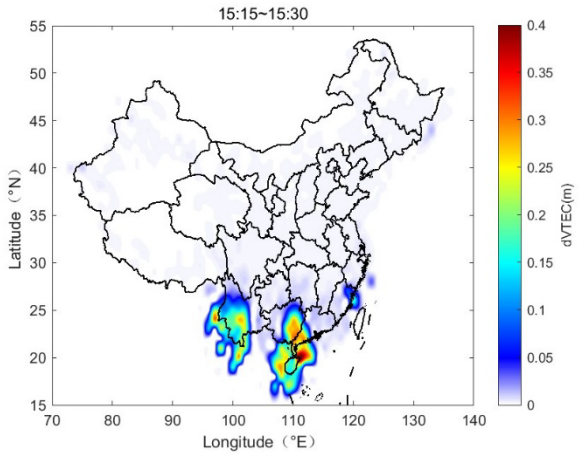


**Figure 5** The geographic distribution of detrended ionospheric residuals over China at 15:15 UTC (23:15 LT).

### 3.3 Results on ionospheric spatial analysis

We displayed the ionospheric spatial correlation of IPPs at the region of [15, 30 °N], [30, 40 °N], and [40, 55 °N] in Figure 6. The figure reflects the ionospheric residuals dependence on the distance. The horizontal and vertical axis is the bins of distances and the delay differences between IPPs. It is a two-dimensional histogram counting the numbers that falls into the bins. Here, the bin resolution for distances and residuals is 10 km and 0.01 m.

The 68%, 95%, 99%, and 99.9% values for bounding the ionospheric spatial residuals are shown in Figure 7. The plotted value is to project them down to the equivalent standard deviation by divided of 1.0, 2.0, 2.58, and 3.29. If the values are close to each other, it shows that the spatial residuals are linearly dependent on distances. Otherwise, it is not.

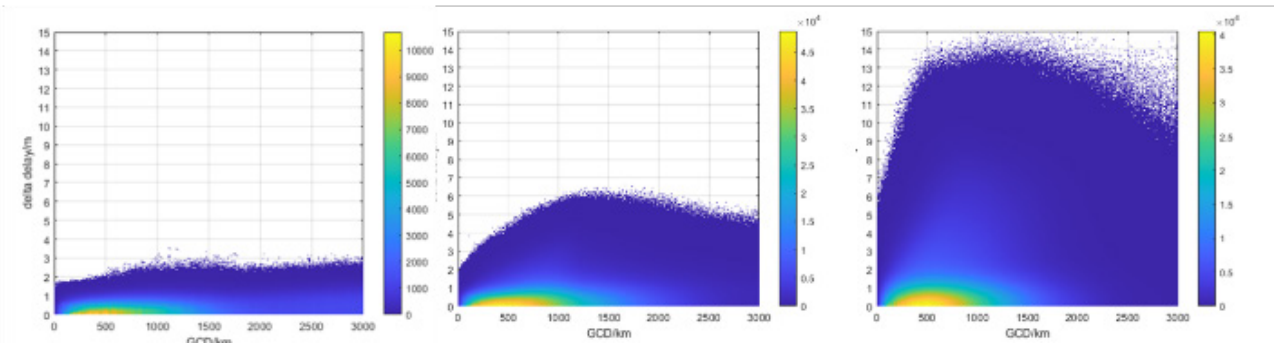


**Figure 6** Ionospheric spatial residuals of IPPs at the region of [40,55°N], [30, 40 °N], [15,30 °N].

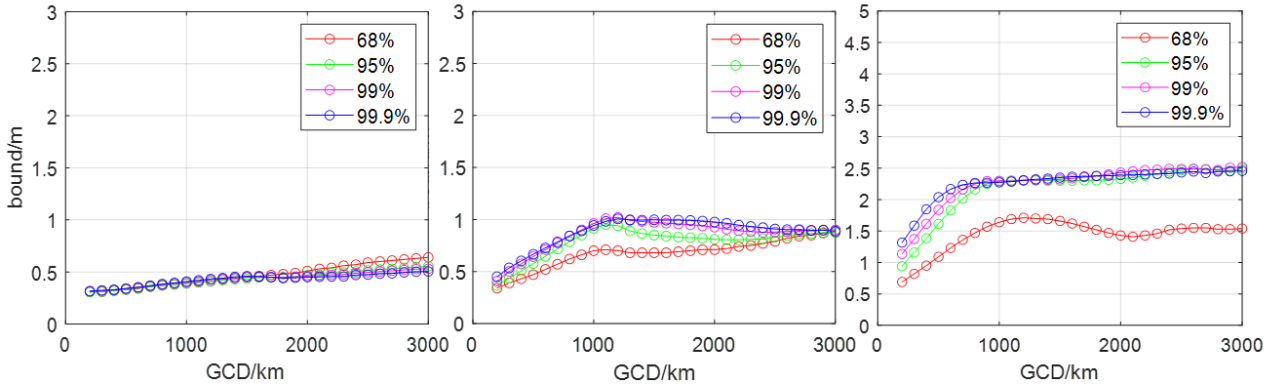


**Figure 7** The 68%,95%, 99%, and 99.9% values for bounding the ionospheric spatial residuals.

Generally, we can see that the ionospheric spatial residuals grow with the distance. In other words, the spatial correlation decreases with the increase in distance. But the spatial correlation showed different patterns at the three different latitude regions.

In the [40, 55 ºN] areas, the areas were the most coherent following the linear pattern. It reaches the plateau around 1000 km to 1500 km. And the ionospheric errors between two IPPs are bounded within 0.5 meters with a high percentile.

In the [30, 40 ºN], [15,30 ºN] areas, the spatial residuals between IPPs displayed a large discrepancy, especially for 68%. The error bounded are much larger compared with the [40, 55 ºN] areas. The error bounds reached as large as 2.5 meters, 5 times larger than the Northern areas. This is also the reason why it is challenging to model the ionospheric delays due to complex spatial variations. The distance is not the only factor and feature contribute to the discrepancies.

## 4. SUMMARIES

The manuscript attempted to investigate the statistics of ionosphere temporal and spatial correlation distributed in China. Clear sunset enhancement and ionospheric scintillation at midnight were identified. Nigh time enhancement was typically around 12:00 UTC (20:00 LT). The scintillation occurred at about 15:00 UTC (23:00 LT).

The unbiased vertical ionospheric delays from the northern, central, and southern areas were presented. The low latitude vertical ionospheric delays were almost four times larger than those from the north. The results confirmed that the TEC peaks around the 25º geographic latitude. The ionospheric delays at the middle latitude stations presented the largest discrepancies for the signals from the directions of south than those from the north.

From the perspective of spatial analysis, the vertical ionospheric delays peak at around geographic latitude of 25 degree, which is almost four time larger than that from the north. In the [30, 40 ºN], [15,30 ºN] areas, the spatial residuals between IPPs displayed a large discrepancy. The error bounded are much larger compared with the [40, 55 ºN] areas. The error bounds reached as large as 2.5 meters, 5 times larger than the Northern areas.

The methods and results presented in this paper benefits the future study of space weather and effects on GNSS positioning in China. And studies on how to handle the unmodeled ionospheric errors and scintillation merit further investigation.

## ACKNOWLEDGMENT

We acknowledge the funding of the National Key R&D Program of China (No. 2021YFB3901301).

## REFERENCES

Jin B, Chen S, Li D, Takka E, Li Z, Qu P (2020) Ionospheric correlation analysis and spatial threat model for SBAS in China region. Advances in Space Research 66(12):2873-2887 doi:10.1016/j.asr.2020.05.010

Li W, Song S, Zhou W, Cheng N, Yu C (2022) Investigating the Impacts of Ionospheric Irregularities on Precise Point Positioning Over China and Its Mechanism. Space Weather 20(11) doi:10.1029/2022sw003236

Luo X, Du J, Lou Y, Gu S, Yue X, Liu J, Chen B (2022) A Method to Mitigate the Effects of Strong Geomagnetic Storm on GNSS Precise Point Positioning. Space Weather 20(1):e2021SW002908 doi:https://doi.org/10.1029/2021SW002908

Lyu S, Xiang Y, Zhang Y, Yang h, Pei L, Yu W, Truong T-K (2023) A consistent and grid-based regional slant ionospheric model with an increasing number of satellite corrections for PPP-RTK. GPS solutions 27(3) doi:https://doi.org/10.1007/s10291-023-01439-z

Marini-Pereira L, Pullen SP, de Oliveira Moraes A (2021) Reexamining Low-Latitude Ionospheric Error Bounds: An SBAS Approach for Brazil. IEEE Trans Aerosp Electron Syst 57(1):674-689 doi:10.1109/taes.2020.3029623

Montenbruck O, Hauschild A, Steigenberger P (2014) Differential code bias estimation using multi - GNSS observations and global ionosphere maps. Navigation 61(3):191-201

Nguyen VK, Rovira-Garcia A, Juan JM, Sanz J, González-Casado G, La TV, Ta TH (2019) Measuring phase scintillation at different frequencies with conventional GNSS receivers operating at 1 Hz. Journal of Geodesy 93(10):1985-2001 doi:10.1007/s00190-019-01297-z

Nie W, Rovira-Garcia A, Wang Y, Zheng D, Yan L, Xu T (2022) On the Global Kinematic Positioning Variations During the September 2017 Solar Flare Events. Journal of Geophysical Research: Space Physics 127(8):e2021JA030245 doi:https://doi.org/10.1029/2021JA030245

Xiang Y, Chen X, Pei L, Luo Y, Gao Y, Yu W (2022) On Enhanced PPP with Single Difference Between-Satellite Ionospheric Constraints. Navigation 69(1)

Xiang Y, Gao Y, Shi J, Xu C (2019) Consistency and analysis of ionospheric observables obtained from three precise point positioning models. Journal of Geodesy 93(8):1161-1170 doi:10.1007/s00190-019-01233-1

Xiang Y, Xu Z, Gao Y, Yu W (2020) Understanding the long-term variations in GPS differential code biases. GPS Solutions 24(118)